Proceedings of the 21st ICSMGE, Vienna, Austria, 14 – 19 June 2026. Pistrol, Adam & Schweiger (eds.)
Published by: ÖGG, Austrian Society for Geomechanics, Salzburg, Austria, ISBN 978-3-9503898-4-5
https://doi.org/10.53243/ICSMGE2026-1527

Dynamic analysis of accelerated post-earthquake ground settlement in the 2023 Kahramanmaraş earthquake sequence

Patrick Bassal, Chong-You Wang, Demián D. Gómez, Charles K. Toth
The Ohio State University, Columbus, OH, USA, bassal.3@osu.edu

ABSTRACT: In the months following the 2023 Kahramanmaraş earthquake sequence (KES), the port city of İskenderun, Türkiye experienced frequent coastal flooding due to ground settlement over shoreline soils. Furthermore, remote sensing observations from Interferometric Synthetic Aperture Radar (InSAR) data reveal increased rates of ground settlement after the mainshock, which may indicate a heightened risk of future flood exposure. Subsurface geotechnical data from borings and cone penetration tests (CPTs) indicate silty sand fills overlying an over 30-meter-thick sequence of soft clays across İskenderun. While the initial co-seismic settlement is primarily attributed to the liquefaction-induced reconsolidation of the silty sands, the mechanism contributing to post-seismic increases in settlement rates remains unclear. To better decipher this phenomenon, this study first evaluates Small-Baseline Subset (SBAS) InSAR displacement rates before and after the KES. These observations are then compared to a nonlinear dynamic analysis (NDA) of a representative uniformly layered site in İskenderun. The NDA is performed using the FLAC2D finite-difference program, with the PM4Sand and PM4Silt constitutive models, which are calibrated against available geotechnical data. Due to current limitations of PM4Silt, the NDAs are integrated with a laboratory-based empirical approach to estimate the post-seismic settlement of the clay soils. This case study demonstrates the potential significance of clay recompression for accelerating post-seismic settlements in İskenderun for over six months after the KES, as observed from both the SBAS InSAR displacement rates and integrated NDA approach. The results also show a mismatch in settlement rates over a longer timeframe of two years after the KES, suggesting needed improvements in NDA approaches and InSAR interpretations of concurrent geophysical and anthropogenic processes.

KEYWORDS: Earthquake, Soil Dynamics, Settlement, Remote Sensing, Finite Difference Method.

1 INTRODUCTION

The 6 February 2023 Kahramanmaraş earthquake sequence (KES) in Türkiye produced severe ground deformations throughout the port city of İskenderun, including damage to pipelines and coastal structures, ground and building settlement, and shoreline lateral spreading. The largest events felt in İskenderun were the M_w7.8 Pazarcık mainshock of the KES, and a M_w6.4 aftershock on 20 February. For about one year after the earthquakes and prior to rehabilitation efforts, the coastline was frequently inundated following modest storms and high tide events (e.g., Moug et al. 2023; CAEES 2024). Flood inundation often extended over 200 m from the shoreline (e.g., Figure 1). Furthermore, temporal trends from interferometric synthetic aperture radar (InSAR) measurements indicated İskenderun's shoreline continued to settle at an unusually accelerated rate from typically under 5-7 cm/yr before the earthquakes to 10-13 cm/yr on average over three months after the earthquakes (Bassal et al. 2024).

The cause and longevity of accelerated ground settlement have remained unclear and could indicate a heightened risk of future flood exposure. The ground deformations and subsequent floods in İskenderun have been primarily attributed to the liquefaction of shoreline fills (e.g., Taftsoglou et al. 2023; Moug et al. 2024; Tobita et al. 2024). However, liquefaction is not typically expected to have a long-term effect on ground settlement rates as observed from the InSAR data. Recent subsurface investigations by Arnold et al. (2025) indicate thick, soft clay deposits underlying the liquefiable silty sands. This work seeks to understand the contribution of these clays to the observed ground displacements.

There is evidence of accelerated rates of post-earthquake settlement over soft clay deposits in the 1995 Kobe and 2011 Tohoku earthquakes, among others (e.g., Matsuda & Shimizu 1996; Yasuhara & Kazama 2015). Increased clay settlement rates have also been observed in several laboratory studies (e.g., Ohara & Matsuda 1988; Fiegel et al. 1998). Although uncommon, some early empirical approaches have been proposed to evaluate post-earthquake clay settlement (e.g., Matsuda & Ohara 1990; Yasuhara et al. 2001). However, there remains a need to better understand this phenomenon and improve modeling efforts relative to case histories.

This work provides a preliminary assessment of the amount and rate of post-earthquake soil settlement in İskenderun. Available historic, geodetic, and geotechnical site data is first introduced. Displacement rates from InSAR data using the Small-Baseline Subset (SBAS) method are then interpreted for alternative time periods before and after the KES. Nonlinear dynamic analyses (NDAs) for a representative site with cone penetration test (CPT) data are next performed. The NDA results are re-evaluated with an empirical approach for post-earthquake clay recompression and compared against the InSAR-based displacement rates. The potential clay contribution to observed displacements and study limitations are discussed.

Figure 1. Flooding in İskenderun on March 29, 2023, about 200 m inland of CPT-IS-48 (Photo by P. Bassal; 36.5912N, 36.1698E).

2 SITE AND SUBSURFACE CONDITIONS

İskenderun is situated in a low-lying coastal floodplain along the eastern shoreline of İskenderun Bay in the Mediterranean Sea, about 20 km west of the East Anatolian fault that ruptured in the 2023 KES. The area was covered by marshes prior to the city's development over the last two centuries. Figure 2 indicates the locations of a major drainage channel in 1901,

swamp ponds in 1916, and the 1916 and 1969 shoreline extents as obtained from historic maps and satellite imagery (Nalça 2018; Taftsoglou et al. 2023).

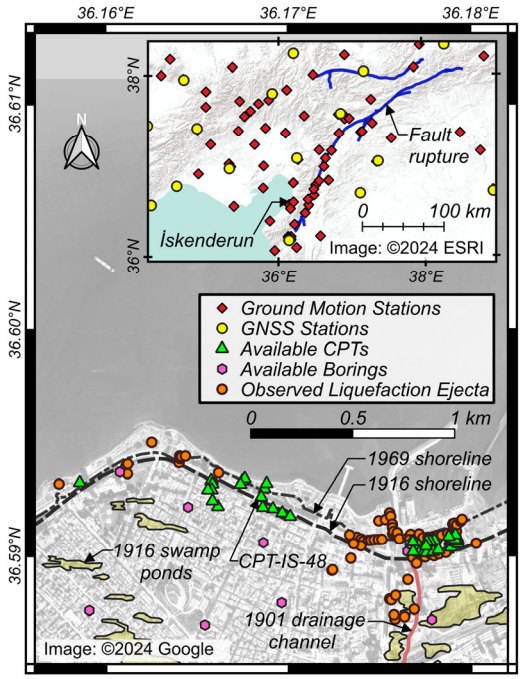

Figure 2. Map of İskenderun with features considered in this study.

A geotechnical investigation was performed in March 2024 that included 40 CPTs and 7 seismic CPTs (SCPTs) pushed along the shoreline as mapped in Figure 2 (Arnold et al. 2025; data available from Macedo et al. 2025). These CPTs were primarily located near buildings that settled, in areas of lateral spreading, and near liquefaction ejecta observed by reconnaissance teams (Figure 2). The CPTs used a 10 cm^2 probe and typically extended to depths of 30 to 43.5 m. Several borings, pressuremeter tests, surface wave tests, and lab tests were also made available to the authors from local studies by Denge Muhendislik Ltd. (2011) and Bayindırlik Zemın Müh (2024). The data indicate groundwater depth in the shoreline area varied from about 1 to 2 m before the KES, and was about 0.5 m shallower after the KES as presumably due to post-earthquake ground settlement and flooding.

The NDA evaluations in this work are conducted for a site located near Emekliler Park along Ataturk Boulevard at CPT-IS-48. This CPT was chosen due to its central location along the shoreline and representative "coarsening upward" soil layering, as also observed in nearby CPTs. This CPT is located just outside an area that experienced liquefaction-induced lateral spreading during the Pazarcık mainshock (Bassal et al. 2024) and was inundated during post-earthquake floods.

Figure 3 plots the corrected cone tip resistance (q_t) and soil behavior type index (I_c) (Robertson 2010) of CPT-IS-48 up to its maximum depth of 43.46 m. The q_t was corrected for measured pore pressures with an assumed net area ratio of 0.80. The indicated soil strata boundaries considered in this study align with visually determined contrasts in q_t and I_c. Stratum A indicates the upper 3 m of pre-drilled material which was primarily clayey gravel. Strata B and C are clean to silty sands extending 9 m and 14 m deep, respectively. Stratum D is a 2-m-thick transitional clayey silt. Strata E and F are soft clay observed in CPTs and borings throughout the city. Stratum F is distinguished from E by the presence of thin interbedded lenses. The ground water table during the CPT push was determined as 0.5 m from pore pressure dissipation tests. Although the CPT did not explore the full extent of Stratum F, a stiff contrast is estimated at 50 m below ground based on nearby microtremor measurements and deep borings (Denge Muhendislik Ltd. 2011; Ozener et al. 2024).

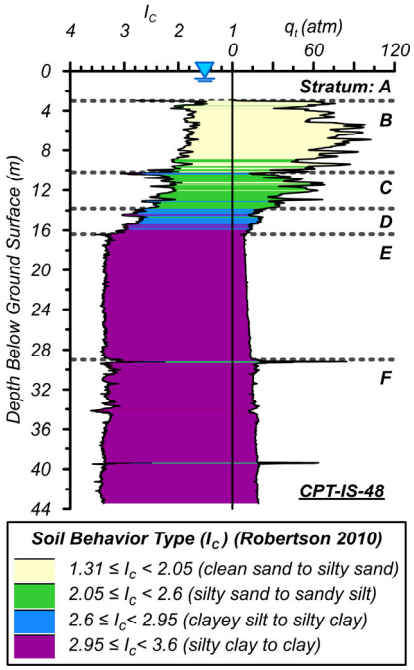

Figure 3. Profile of I_c and q_t for CPT-IS-48 with the labeled stratum delineations used in this study.

3 DISPLACEMENT RATES FROM REMOTE SENSING

3.1 *InSAR processing*

The remote sensing evaluations used two frames of pre-processed interferograms from ascending and descending tracks provided by LiCSAR dataset (Lazeckỳ et al. 2020), which processes Sentinel-1A and -1B interferometric wide mode SAR images by GAMMA (Wegnüller et al. 2016). Line-of-sight (LOS) surface displacements between February 2021 and February 2025 were derived using the SBAS method (Morishita et al. 2020). To prevent decorrelation associated with the earthquake, we conducted the InSAR processing for pre-seismic (Feb2021 to Feb2023) and post-seismic (Feb2023 to Feb2025) periods and excluded the interferograms involving the KES on 6 February 2023. The reference point for InSAR measurements was chosen at ground motion recording station TK3115, which is near the city (i.e., ~5 km south of the shoreline) and located over stiff soils. This helped remove other broad-scale geophysical processes, such that the InSAR measurements primarily reflect local settlement deformation. The spatial resolution of InSAR observations is 100 m. The InSAR measurements with average coherence higher than 0.3 were selected for further analysis.

3.2 *Estimation of LOS displacement rate*

During the pre-seismic period, the LOS displacement rates are estimated using the trajectory model (Bevis and Brown 2014) as follows:

$$D(t) = x_{ref} + v\left(t - t_{ref}\right) + \sum_{k=1}^{2} s_k \sin(\omega_k t) + c_k \cos(\omega_k t) \quad (1)$$

where $D(t)$ is the LOS time series of displacements, x_{ref} is the displacement at reference epoch t_{ref}, and v is the displacement rate. The reference epoch t_{ref} is set to the first SAR acquisition

date. A four-term Fourier series is used to account for annual and semi-annual trends (e.g., seasonal patterns), where s_k and c_k are the Fourier coefficients and ω_k is the angular frequency. The parameters are solved by the least-square method.

For the post-seismic period, we modified the trajectory model to incorporate the short-term (Feb2023-July2023) and long-term (July2023-Feb2025) displacement rates:

$$D(t) = x_{ref} + v_1(t - t_{ref})h_1(t, t_{ref}) + v_2(t - t_{ref})h_2(t, t_{ref}) + \sum_{k=1}^{2} s_k \sin(\omega_k t) + c_k \cos(\omega_k t) \quad (2)$$

$$h_1(t, t_{ref}) = \begin{cases} 0 & \text{if } t \geq t_{ref} \\ 1 & \text{if } t < t_{ref} \end{cases} \quad (3)$$

$$h_2(t, t_{ref}) = \begin{cases} 1 & \text{if } t \geq t_{ref} \\ 0 & \text{if } t < t_{ref} \end{cases} \quad (4)$$

where v_1 and v_2 are short-term and long-term displacement rates and are controlled by the unit step functions h_1 and h_2. Here t_{ref} is chosen in early July, due to a prominent change in displacement rate and to facilitate comparisons in this study.

3.3 *Estimation of vertical displacement rates*

The LOS displacement rates during pre-seismic, short-term post-seismic, and long-term post-seismic periods are further decomposed to vertical displacement rates to reflect settlement. Benefitting from the different viewing geometries of ascending and descending SAR images, LOS displacement rates were decomposed into east-west v_e and vertical v_v directions by:

$$\begin{bmatrix} v_e \\ v_v \end{bmatrix} = \begin{bmatrix} -\cos(\varphi_{asc})\sin(\theta_{asc}) & \cos(\theta_{asc}) \\ -\cos(\varphi_{des})\sin(\theta_{des}) & \cos(\theta_{dec}) \end{bmatrix}^{-1} \begin{bmatrix} v_{asc} \\ v_{des} \end{bmatrix} \quad (5)$$

where φ and θ are azimuth and incidence angles of the InSAR pixel, respectively. The v_{asc} and v_{des} are the LOS displacement rates from ascending and descending data, as estimated by Equations (1) and (2). The decomposition assumes that north-south deformations contribute insignificantly to the LOS measurements. This assumption is generally valid, given that Sentinel-1 operates in near-polar orbit and is thus insensitive to north-south motions. In addition, although liquefaction-induced lateral spreading can cause north-south motion, settlement is the dominating signal in the study area. Consequently, the north-south displacements are expected to be minor and do not affect the estimation of vertical displacements.

3.4 *Results*

The pre-seismic, short-term post-seismic, and long-term post-seismic vertical displacement rates are shown in Figure 4. Prior to the earthquake, the settlement rates in the city range from -70 to -20 mm/yr (note that negative values indicate downward settlement). During the first 6 months after the earthquake, the subsiding region extends along the coastline, and exhibits a rapid drop ranging from -250 to -50 mm/yr. After July 2023, vertical displacements in the city appear to stabilize, with slight uplift in areas south of the shoreline.

The displacements at the location of CPT-IS-48 were determined from the nearest coherent InSAR observations about 200 m away. During the three periods, the vertical displacement rates at CPT-IS-48 are -20.6, -96.9, and -3.3 mm/yr, respectively. The LOS displacement time series data in Figure 5 from ascending and descending data show similar trends. Both time series are nearly flat after July 2023, which may imply the region is no longer settling.

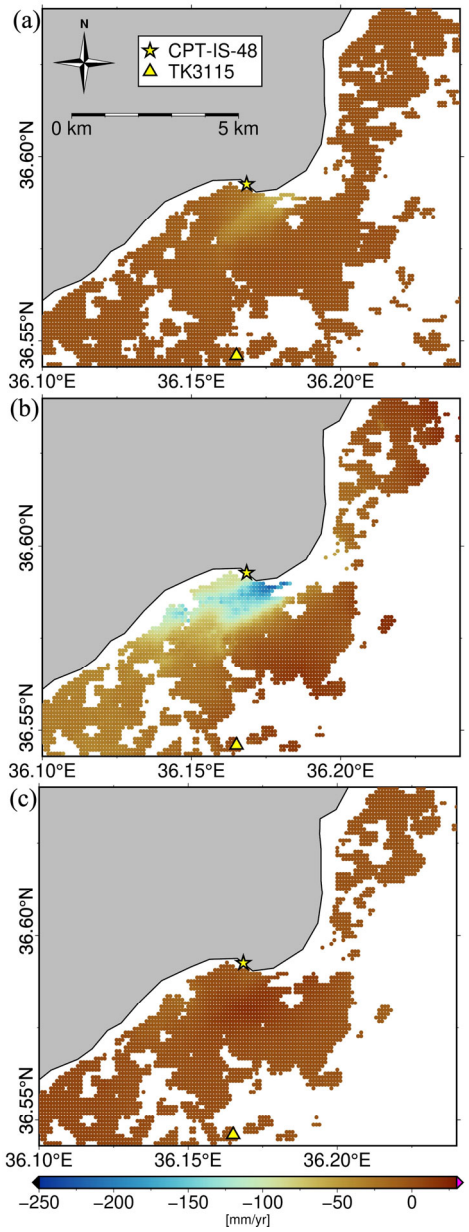

Figure 4. SBAS maps of vertical displacement rate for three time periods: (a) pre-earthquake (Feb2021 to Feb2023), (b) short-term post-earthquake (Feb2023 to July2023), and (c) longer-term post-earthquake (July2023 to Feb2025).

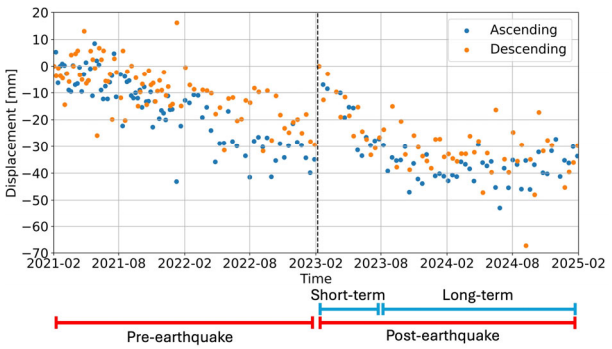

Figure 5. LOS displacement time series at CPT-IS-48 from (a) ascending and (b) descending Sentenel-1 SAR data. Semi-annual and annual trends are removed from the time series. Displacements are relative to 0 at the start of the pre- and post-earthquake periods.

4 NONLINEAR DYNAMIC ANALYSIS

4.1 *Representative Soil Properties*

An NDA was performed for a soil column at CPT-IS-48 using the FLAC2D v9.4 (Itasca 2025) finite difference program to evaluate shaking-induced soil settlement. The single column mesh was constructed with the soil strata divisions in Figure 3. The mesh is 1-m-wide by 51-m-deep, and consists of 0.5-m-thick elements. The 50-m-deep soil column is underlain by a 1-m-thick "base" material representing an elastic halfspace.

Representative properties were selected for each stratum as indicated in Table 1. The saturated unit weight (γ_{sat}) was estimated from nearby borings as 18 kN/m^3 for all soil strata, and 20 kN/m^3 for the base material. A unit weight of 17 kN/m^3 was assigned above the water table by enforcing a lower porosity for unsaturated elements. The shear wave velocity (V_s) in each stratum was approximated from nearby SCPT-13 by Macedo et al. (2025) and surface wave measurements by Tobita et al. (2024). The vertical permeability (k_v) was estimated from I_c correlations by Robertson (2010). For sand-like Strata B and C, the median stress-normalized clean sand-corrected tip resistance (q_{c1Ncs}) was determined per Boulanger & Idriss (2014), with liquefaction defined at I_c=2.6 and a percentile-weighted fines content correction by Bassal et al. (2022) from local boring data. Gravelly fill Stratum A assumed q_{c1Ncs}=125. For clay-like Strata D, E, and F, the median undrained shear strength (s_u) and ratio term (s_u/σ'_{vc}) were calculated with a cone bearing factor (N_{kt}) of 16, as calibrated to local pressuremeter and triaxial tests, and corrected for direct simple shear conditions. Strata E and F have over-consolidation ratios of 1.05-1.30, and were checked to not have significant "organic" or "sensitive" tendencies per Mayne et al. (2025).

Table 1. Representative soil properties selected for NDA.

Str.	γ_{sat} (kN/m^3)	V_s (m/s)	k_v (m/s)	q_{c1Ncs}	s_u (kPa)	s_u/σ'_{vc}
A	18	170	1E-5	125	-	-
B	18	200	1E-5	93	-	-
C	18	200	1E-6	92	-	-
D	18	215	3E-8	-	76	-
E	18	205	1E-9	-	-	0.22
F	18	230	1E-9	-	-	0.22
Base	20	400	1E-9	-	-	-

4.2 *Co- and Post-Seismic Modeling Approach*

The NDA allowed soil-fluid coupling via Biot's theory of poroelasticity and was executed in two stages: (1) co-seismic, and (2) post-seismic. The user-defined constitutive soil models PM4Sand Version 3.3 and PM4Silt Version 2.1 (Boulanger and Ziotoupolou 2023a; 2023b) were employed to evaluate liquefaction behavior in sand-like soils and cyclic softening in clay-like soils, respectively, for both stages of analysis.

For the co-seismic stage, stress conditions were first initialized for a lateral earth pressure coefficient of 0.5 for all strata. The water table was initialized at 1 m deep, to approximate pre-earthquake boring observations (i.e., prior to settlement and flooding), with saturation held constant during modeling. Periodic (i.e., attached) boundaries were assumed at the sides of the mesh, and an outcropping ground motion was input at a compliant base as a horizontal stress time history.

The north-oriented TK3115 Pazarcık recording with a peak ground acceleration of PGA=0.29g (Buckreis et al. 2023) was applied at the model base. TK3115 is 5 km south of CPT-IS-48, with V_s in the upper 30 m (V_{s30}) of 424 m/s, which is consistent with stiff layers below site Stratum F, reducing potential site effects. The site and station are both about 18 km away from the fault rupture, reducing potential path effects. The motion was cropped over an effective duration of 100 s and baseline corrected by linear detrending. The 20 February aftershock is not considered due to its relatively low M_w and PGA.

For the post-seismic stage, following the duration of the ground motion, the "post-shake" option of the PM4 models was assigned to all soil elements to estimate volumetric reconsolidation. Porewater pressures were fixed at the model base to prevent downward porewater drainage. The k_v was scaled up in all elements by a factor of 10^3, and modeling resumed for an additional 86.4 seconds of flow time, or 24 hours in real time. The k_v in Strata C, D, E, and F was then scaled up by an additional 10^3 factor and modeling resumed for an additional 157.8 seconds of flow time, or 5 years in real time.

PM4Silt cannot directly model the recompression behavior of clays. Post-earthquake clay settlement was thus also assessed using the lab-based empirical approach by Yasuhara et al. (2001) to allow recompression during porewater dissipation as observed in dynamic triaxial tests on Drammen clay. This approach assumes a post-earthquake recompression rate ($C_{r,eq}$) of 0.225 times the static virgin compression rate (C_c) to determine the post-earthquake clay recompression (S_{vr}):

$$S_{vr} = \int_0^{z_{max}} 0.225 \left(\frac{2.3\sigma'_{vc}}{M}\right) \log\left(\frac{1}{1-r_u}\right) dz \qquad (6)$$

where M is the oedometer modulus as estimated from the CPT per Robertson (2009), σ'_{vc} is the initial vertical effective stress, r_u is the excess pore pressure ratio (i.e., determined from the NDA herein as one minus the ratio of current to initial effective stress), dz is the depth increment along the CPT, and z_{max} is the max depth considered. For this study, the median M of Stratum F was extrapolated below the CPT to z_{max} = 50 m.

The average time rate of settlement was approximated using the Terzaghi 1D consolidation theory. The drainage length was approximated as 17.5 m to roughly account for dissipation at thin interbedded lenses. The coefficient of consolidation (c_v) was determined from the overall median of M and the $C_{r,eq}$ rate as:

$$c_v = \left(\frac{M}{0.225}\right)\left(\frac{k_v}{\gamma_w}\right) \qquad (7)$$

where γ_w is the unit weight of water or 9.81 kN/m^3.

4.3 *Constitutive Model Calibrations*

The PM4Sand and PM4Silt input parameters presented in Table 2 and Table 3 were developed using calibration protocols detailed for previous NDA case histories by the first author (e.g., Bassal & Boulanger 2023). Strata A, B, and C were modeled with PM4Sand with data-based correlations for the relative density (D_R) and shear modulus coefficient (G_o). Contraction rate parameter h_{po} was calibrated using a magnitude-standardized cyclic resistance ratio ($CRR_{M7.5}$) for a 50% probability of liquefaction. Secondary parameter C_ε was adjusted for Stratum A to allow reasonable strain accumulation rates for a low σ'_{vc}. Strata D, E, and F were modeled with PM4Silt with earthquake rate- and critical state-adjusted shear strength terms $s_{u,cs,eq}$ and $s_{u,cs,eq}/\sigma'_{vc}$. A factor of 1.25 was applied to all strata to account for earthquake loading rate strength gains, and a peak-to-critical state ratio reduction factor of 0.67 was applied to Strata E and F to account for monotonic softening. Parameters G_o, h_o, h_{po}, and $n_{b,wet}$ were obtained per the mentioned protocols. Post-earthquake elastic modulus degradation factor c_{hg} was set at 1000 to maximize recompression strains in the NDA.

Table 2. PM4Sand constitutive model inputs.

Str.	D_R	G_o	σ'_{vc} (atm)	$CRR_{M7.5}$	h_{po}	C_ε
A	0.647	1200	0.30	0.246	0.24	1.5
B	0.519	1140	0.60	0.165	0.37	-
C	0.512	907	1.06	0.154	0.74	-

Table 3. PM4Silt constitutive model inputs.

Str.	$s_{u,eq,cs}$ (kPa)	$s_{u,eq,cs}/\sigma'_{vc}$	G_o	σ'_{vc} (atm)	h_{po}	h_o	$n_{b,wet}$
D	95.3	-	928	1.31	40	1.0	-
E	-	0.186	632	1.92	18	1.2	0.37
F	-	0.186	534	3.27	25	0.8	0.40

4.4 *Results*

The co-seismic and post-seismic CPT-IS-48 responses with depth for the NDA with the PM4Silt post-shake option are presented in Figure 6. Figures 6a-c depict maximum values during shaking for the cyclic stress ratio (CSR), r_u, and engineering shear strain (γ_{xy}). The max r_u is about 100% through Stratum B, indicating liquefaction triggering. This is also indicated by γ_{xy} of up to 4% in Stratum B. The Strata E and F clays indicate an r_u range of 25% to 30% and γ_{xy} range of 0.12 to 0.32%. This range of pore pressure development is consistent with cyclic simple shear tests of Kaolinite clays by Ohara & Matsuda (1988). Figure 6d depicts vertical displacements relative to the bottom of the 50-m-deep profile immediately, 24 hours, and 5 years after shaking. Less than 1 cm of displacement occurs during shaking. At 24 hours, the settlement is 11 cm, which is primarily due to volumetric compression in liquefied Stratum B. This underestimates inferences of 25 to 50 cm of shoreline settlement observed relative to nearby pile-founded coastal structures (e.g., Tobita et al. 2024, CAESS 2024). At 5 years, only 2.5 cm of additional settlement is modeled due to compression of clay Strata E and F.

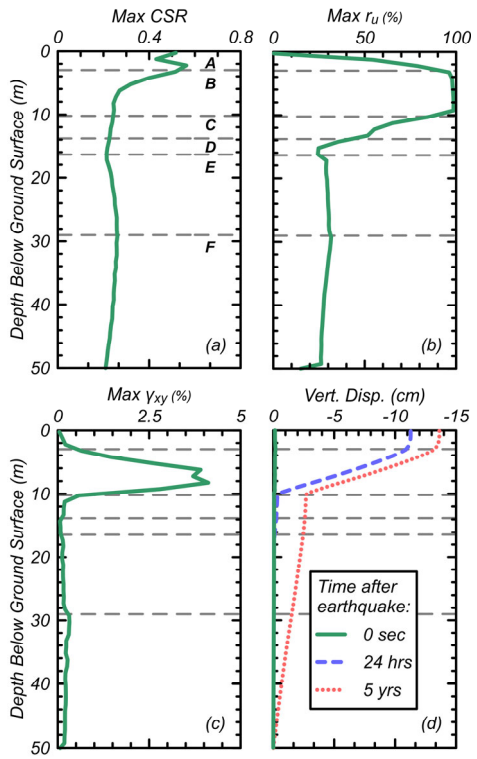

Figure 6. NDA profile results at CPT-IS-48 for: (a) maximum CSR, (b) maximum r_u, (c) maximum γ_{xy}, and (d) vertical displacement. The post-earthquake displacements are for the PM4Silt "post-shake" option.

Figure 7 depicts time histories of r_u and ground settlement for selected points over three intervals: 100 s of shaking, 24 hours after shaking, and 5 years after shaking. The r_u histories in Figure 7a show that the center of Stratum B approaches a liquefied state about 44 s into shaking, and excess pore pressures take about 8 hours to dissipate. The center of Stratum F approaches its maximum r_u at about 60 s and takes nearly 4 years to fully dissipate.

The settlement histories in Figure 7b indicate results from (1) the NDA with the PM4Silt "post-shake" option, and (2) the NDA integrated with the clay recompression empirical approach (Equations 6 and 7). The PM4Silt "post-shake" option indicates 2.5 cm of settlement over 5 years, consistent with Figure 6d. However, the NDA-empirical approach indicates a total clay recompression of S_{vr}=19.9 cm in Strata E and F, in addition to liquefaction settlement. As determined from the Terzaghi consolidation theory, 6.0 cm of S_{vr} occurs at 6 months, 12.1 cm at 2 years, and 17.4 cm at 5 years. Simplifying assumptions with the Terzaghi theory (e.g., infinite water modulus, 1D flow, average drain length) could indicate a slower consolidation rate relative to the Biot theory used by the NDAs. Nonetheless, the NDA-empirical approach herein considers lab-observed clay recompression processes that are unaccounted for by PM4Silt, and can provide a more realistic prediction of post-earthquake settlement.

The SBAS observations and NDA predictions of post-earthquake settlement are compared in Table 4. Six months after the KES, the NDA-empirical approach only slightly overpredicts the SBAS settlement of 4.8 cm. However, SBAS indicates an additional settlement of only 0.5 cm at 2 years, which is much lower than the NDAs for this time interval and could imply other stabilizing processes not considered. This may include changes in groundwater and land use during post-seismic recovery, local tectonic movements, and other effects.

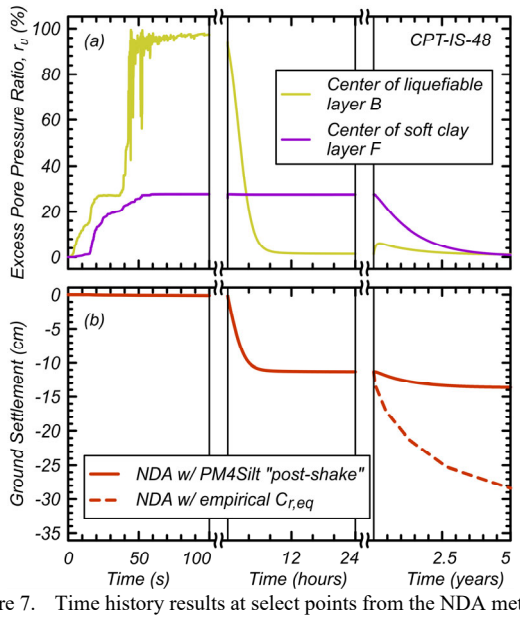

Figure 7. Time history results at select points from the NDA methods for CPT-IS-48 of (a) r_u, and (b) ground settlement. The 0 to 100 s period is the time during earthquake shaking.

Table 4. Summary of post-earthquake settlement from SBAS observations and NDAs at CPT-IS-48.

Method	Settlement 6 months after KES (cm)	Settlement 2 years after KES (cm)
InSAR (SBAS)	4.8	5.3
NDA w/ PM4Silt "post-shake"	0.7	1.9
NDA w/ empirical $C_{r,eq}$	6.0	12.1

5 CONCLUSIONS

This study compared displacement rates from SBAS InSAR and NDA approaches to evaluate the contribution of clay recompression for accelerating ground settlement near CPT-IS-48 in İskenderun following the 2023 KES. Over 2 years before the KES, pre-seismic SBAS observations indicated ~2 cm/yr of steady settlement. Over 6 months after the KES, the SBAS settlement rates significantly increased to ~10 cm/yr, similar to predictions from the NDA integrated with empirical adjustments for clay recompression. Over 6 months to 2 years after the KES, the SBAS rates nearly stabilize, whereas the integrated NDA-empirical approach suggests continued settlement at a decaying rate.

These findings suggest the potential significance of clay recompression for accelerating short-term settlements in İskenderun. The NDA results highlight the need for improved models that more directly accommodate post-earthquake clay recompression processes. Comparisons of settlement rates from InSAR and NDAs suggest a need for improved interpretations of concurrent geophysical and anthropogenic processes. Further evaluations of spatial settlement patterns and an extended monitoring period can provide additional insights.

6 ACKNOWLEDGEMENTS

The field reconnaissance and data collection for the case study were supported by the National Science Foundation (NSF) (awards CMMI 1826118 and CMMI 2338026). The first author is grateful for collaborations on various aspects of this case study with Diane Moug, Jon Bray, Jorge Macedo, K. Onder Cetin, Elena Papageorgiou, Cody Arnold, Fikret Atalay, and Murat Bikçe. Any opinions, findings, conclusions, or recommendations expressed in this material are those of the authors and do not necessarily reflect the views of NSF.

7 REFERENCES

Arnold, C., Macedo, J., Bray, J., Moug, D., Atalay, F., Bassal, P., Liu, C., Bikce, M., & Durgunoglu, T. 2025. Field Characterization of Areas in İskenderun Affected by Liquefaction during the 2023 Kahramanmaraş Earthquake. *Earthq. Spectra*, 0(0). doi.org/10.1177/87552930251378227

Bassal, P. C., & Boulanger, R. W. 2023. System Response of an Interlayered Deposit with a Localized Graben Deformation in the Northridge Earthquake. *Soil Dyn. and Earthq. Eng.,* 165(107668). doi.org/10.1016/j.soildyn.2022.107668

Bassal, P. C., Boulanger, R. W., & DeJong, J. T. 2022. Site-Specific CPT-based Fines Content Correlations using Percentile Matching. *Proc. Geo-Congress*, doi.org/10.1061/9780784484043.053

Bassal, P., Papageorgiou, E., Moug, D. M., Bray, J. D., Cetin, K. O., Sahin, A., Kubatko, E. J., Nepal, S., Toth, C., Kendir, S. B., & Bikçe, M. 2024. Liquefaction Ground Deformations and Cascading Coastal Flood Hazard in the 2023 Kahramanmaras Earthquake Sequence. *Earthq. Spectra*, 40(3). doi.org/10.1177/87552930241247830

Bayindırlik Zemın Müh, 2024. Sami Yildiz-Yildiz Plaza B Block, Reinforcement Project of a Moderately Damaged Building. *Soil and Foundation Survey Report*, Reg. Num.: 17436 (in Turkish)

Bevis, M., & Brown, A. 2014. Trajectory models and reference frames for crustal motion geodesy. *Journal of Geodesy*, 88(3), 283-311.

Boulanger, R. W., & Idriss, I. M. 2015. CPT-based liquefaction triggering procedure. *J. Geotech. Geoenviron. Eng.,* ASCE, 142(2), 04015065, 10.1061/(ASCE)GT.1943-5606.0001388.

Boulanger, R. W., and Ziotopoulou, K. 2023a. PM4Sand (Ver 3.3): A sand plasticity model for earthquake engineering applications. Report No. UCD/CGM-23/01, *Center for Geotech. Modeling, Dept. of Civil and Env. Eng., UC Davis.*

Boulanger, R. W., & Ziotopoulou, K. 2023b. PM4Silt (Ver 2.1): A silt plasticity model for earthquake engineering applications. Report No. UCD/CGM-23/02, *Center for Geotech. Modeling, Dept. of Civil and Env. Eng., UC Davis.*

Buckreis, T.E., Pretell, R., Sandikkaya, M.A., Kale, O., Askan, A., Brandenberg, S.J., & Stewart, J.P. 2024. Engineering attributes of ground motions from February 2023 Turkiye earthquake sequence. *Earthq. Spectra,* 40(4). 10.1177/87552930241259024.

CAEES. 2024. February 6, 2023 Kahramanmaraş Earthquakes in Türkiye Reconnaissance Report. *Canadian Assoc. Earthq. Eng. & Seis.*

Denge Muhendislik Ltd. 2011. Hatay Prov., İskenderun Dist., İskenderun Municipality, Microzonation Report. Antakya, TR.

Fiegel, G. L., Kutter, B. L., & Idriss, I. M. 1998. Earthquake-induced settlement of soft clay. *Proc., Centrifuge 98*, Balkema, Rotterdam (1), pp. 231–36.

Itasca Consulting Group, Inc. (Itasca). 2025. FLAC2D: Fast Lagrangian Analysis of Continua in Two-Dimensions, Ver. 9.4. Minneapolis.

Lazecký, M., Spaans, K., González, P. J., et al. 2020. LiCSAR: An automatic InSAR tool for measuring and monitoring tectonic and volcanic activity. *Remote Sensing*, 12(15), 2430.

Macedo, J., Bray, J., Moug, D., Bassal, P., & Arnold, C. 2025. Subsurface Characterization of İskenderun – 2024. Ver 2. *DesignSafe-CI.* doi.org/10.17603/ds2-6473-fs88

Matsuda, H., & Ohara, S. 1990. Geotechnical Aspects of Earthquake-Induced Settlement of Clay Layer. *Marine Geotechnology*, 9, pp 179-206.

Matsuda, H., & Shimizu, Y. 1996. Seismic ground subsidence in near-shore reclaimed land. *The Kobe Earthquake Geodyn. Aspects, Comp. Mech. Pubs*., Southampton, UK, pp 73-98.

Mayne, P. W., Cargill, E., & Greig, J. 2025. Piezocone Screening Approach for Regular, Organic, and Sensitive Soft Clays. *Proc., ASCE Geo-Frontiers*, Louisville, KY.

Morishita, Y., Lazecky, M., Wright, T. J., Weiss, J. R., Elliott, J. R., & Hooper, A. 2020. LiCSBAS: An open-source InSAR time series analysis package integrated with the LiCSAR automated Sentinel-1 InSAR processor. *Remote Sensing*, 12(3), 424.

Moug, D. M., Bray, J. D., Bassal, P., Macedo, J., Ulmer, K., Cetin, K. O., Kendir, S. B., Şahin, A., Arnold, C., & Bikçe, M. 2024. Liquefaction-Induced Building and Ground Interactions in İskenderun from the 2023 Kahramanmaraş Earthquake Sequence. *Earthq. Spectra*, 40(2). doi.org/10.1177/87552930241232994

Moug, D., Bassal, P., Bray, J. D., Çetin, K. Ö., Kendir, S. B., Şahin, A., Çakır, E., Söylemez, B., & Ocak, S. 2023. February 6, 2023 Türkiye Earthquakes: GEER Phase 3 Team Report on Selected Geotechnical Engineering Effects. *Geotechnical Extreme Events Reconnaissance (GEER) Association*, Report No. GEER-082-S1, 30 June. doi.org/10.18118/G6F379

Nalça, C. 2018. Transformation of İskenderun Historic Urban Fabric from Mid 19th Century to the End of the French Mandate Period. MS Thesis, *Dept of Arch. Rest., İzmir Institute of Tech.*

Ohara, S., & Matsuda, H. 1988. Study on the Settlement of Saturated Clay Layer Induced by Cyclic Shear. *Soils and Foundations* 28, 3, pp 103-113.

Ozener, P., Monkul, M. M., Bayat, E. E., Ari, A., Cetin, K. O. 2024. Liquefaction and performance of foundation systems in İskenderun during 2023 Kahramanmaras-Turkiye earthquake sequence. *Soil Dyn & Eq Eng*, 178 108433.

Robertson, P. K. 2009. Interpretation of cone penetration tests - a unified approach. *Can. Geotech. J.* 46: 1337-1355.

Robertson, P. K. 2010. Soil behaviour type from the CPT: an update. *Proc. 2nd Int. Symp. on Cone Penetration Testing*.

Taftsoglou, M., Valkaniotis, S., Papathanassiou, G., Karantanellis, E. 2023. Satellite Imagery for Rapid Detection of Liquefaction Surface Manifestations: The Case Study of Türkiye-Syria 2023 Earthquakes. *Remote Sensing*, 15, 4190. doi.org/10.3390/rs15174190.

Tobita, T., Kiyota, T., Torisu, S., et al. 2024. Geotechnical damage survey report on February 6, 2023 Turkey-Syria Earthquake, Turkey. *Soils and Foundations*. 64(3) 101463.

Wegnüller, U., Werner, C., Strozzi, T., Wiesmann, A., Frey, O., & Santoro, M. 2016. Sentinel-1 support in the GAMMA software. *Procedia Computer Science*, 100, 1305-1312.

Yasuhara, K., & Kazama, M. 2015. Land subsidence of clay deposits after the Tohoku-Pacific Ocean Earthquake (Keynote Lecture). *Proc. IAHS*, 372, pp. 211-216, doi:10.5194/piahs-372-211-2015

Yasuhara, K., Murakami, S., Toyota, N., & Hyde, A. F. L. 2001. Settlement in fine-grained soils under cyclic loading. *Soils and Fdns, J. of Japanese Geotechnical Society*, 41(6): 25-36.